

# Surface EM waves on 1D Photonic Crystals

G. V. Morozov

*School of Mathematics, University of Bristol  
Bristol, BS8 1TW United Kingdom*

D. W. L. Sprung

*Department of Physics and Astronomy, McMaster University  
Hamilton, Ontario L8S 4M1 Canada*

J. Martorell

*Departament d'Estructura i Constituents de la Materia,  
Facultat Física, University of Barcelona  
Barcelona 08028, Spain*

(Dated: June 27, 2006)

We study surface states of 1D photonic crystals using a semiclassical coupled wave theory. Both TE and TM modes are treated. We derive analytic approximations that clarify the systematics of the dispersion relations, and the roles of the various parameters defining the crystal.

Keywords: photonic crystals, surface waves, semiclassical coupled wave theory

## I. INTRODUCTION

Photonic crystals are artificial low-loss dielectric structures with periodic modulation of refractive index, which have attracted considerable attention in the last two decades. Due to Bragg reflection, electromagnetic (optical) waves cannot propagate through such structures in certain directions, at certain frequencies. Hence, photonic crystals can control the propagation of electromagnetic waves in novel ways, with obvious application to dielectric mirrors, dielectric waveguides, and dielectric laser cavities.

As a way to efficiently inject light into a photonic crystal (PC) waveguide, it has recently been proposed to use surface electromagnetic waves (SEW)[1, 2]. In those papers, the photonic crystal was a two dimensional array of rods, of infinite length normal to the plane of incidence. Instead, we have studied SEW on a semi-infinite one-dimensional (1D) photonic crystal sketched in Fig. 1. While retaining all useful properties of 2D and 3D photonic crystals, a 1D dielectric periodic structure with high refractive index contrast is more attractive from a technological point of view.

The usual theoretical methods for wave propagation in 1D photonic crystals, including SEW, are the Floquet-Bloch modal formalism, coupled wave theory, and the transfer matrix method. Among these three, the coupled wave approach[3, 4, 5] offers superior physical insight and gives simple analytical results in limiting cases. Unfortunately, the conventional coupled wave theory of Kogelnik fails in the case of high refractive index contrast, which is essential for a functional 1D photonic crystal.

In this paper, we apply our recently developed semiclassical version of coupled wave theory[6, 7, 8] to SEW on 1D photonic crystals. The method is analytically almost as simple as conventional coupled wave theory, and is practically exact for the achievable ratios (e.g. 1.5:4.6)

of the indices of refraction of the materials available to build devices. We present here a unified description of TE and TM SEW. A detailed account of the properties of the TE surface modes has recently been given by us in Ref. [9]; here we complement these findings with those for TM modes, which are slightly more complex due to the presence of Brewster points in the bandgaps. As a result, we thoroughly clarify the systematics of solutions for surface EM waves in semi-infinite 1D photonic crystals.

Our method is formally quite different from that recently presented in Ref. [10], or those in Ref. [11], so in Section II we provide a short summary of the transfer matrix approach, in the notation of our previous work[7]. In Section III we rederive the exact equations for SEW of TM modes and obtain from them various analytic approximations for a semi-infinite crystal. The analogous equations for TE modes were given in Ref. [9]. With these in hand, we discuss systematics of SEW. In Section IV we apply the semiclassical approximations of Refs. [7] and [8] to surface waves, and show that the second approximation is very accurate both for the dispersion relation and the bandgap boundaries.

## II. TRANSFER MATRIX METHOD FOR A PERIODIC CRYSTAL

We wish to describe surface states that form at the interface between a medium of low refractive index,  $n_0$ , and a semi-infinite 1-D photonic crystal with layers of refractive indices  $n_1$  and  $n_2$  and thicknesses  $d_1$  and  $d_2$ . We choose a coordinate system in which the layers have normal vector along OZ. As shown in Fig. 1, the crystal is capped by a layer of the same material but different width,  $d_c$ . For convenience of presentation, we split this termination layer of index of refraction  $n_1$  and width  $d_c$

into two sublayers, of lengths  $d_s + d_t = d_c$ . The first sublayer extends from  $z = -d_s$  to  $z = 0$ . Then the periodic array that forms the 1D photonic crystal consists of “cells” each made of three uniform layers of widths  $d_t$ ,  $d_2$  and  $d_1 - d_t$  whose respective indices of refraction are  $n_1$ ,  $n_2$  and  $n_1$ . (If  $d_t = d_1/2$ , the unit cell will have reflection symmetry, which simplifies some relations, but does not change any physical results.) The first cell, given index 0, ranges from  $z = 0$  to  $z = d \equiv d_1 + d_2$ ; the second is given index 1, and ranges from  $z = d$  to  $2d$ , etc. The  $p$ -th cell runs from  $pd$  to  $(p+1)d$  and has  $n(z) = n_1$  when  $pd < z < pd + d_t$  or  $pd + d_t + d_2 < z < (p+1)d$  and  $n(z) = n_2$  when  $pd + d_t < z < pd + d_t + d_2$ . We choose  $n_1 > n_2 > n_0$ .

For monochromatic TE waves the electric field is parallel to the OY axis. As in Ref. [7], we write

$$\mathbf{E} = E_y(z)\hat{\mathbf{e}}_y e^{i(k\beta x - \omega t)}, \quad (1)$$

where  $\omega$  is the angular frequency,  $k = \omega/c$  is the vacuum wavenumber and  $\beta k$  is the (constant)  $x$ -component of the wavevector of modulus  $k(z) = \omega n(z)/c$ . For an electromagnetic wave entering the 1D photonic crystal from a uniform medium, one has

$$\beta = n_0 \sin \theta_0, \quad (2)$$

where  $\theta_0$  is the angle of incidence measured from the normal. For monochromatic TM waves it is the magnetic field which lies parallel to the OY axis. Following Ref. [8], we write

$$\mathbf{H} = H_y(z)\hat{\mathbf{e}}_y e^{i(k\beta x - \omega t)}. \quad (3)$$

For piecewise constant  $\epsilon(z) = n^2(z)$ , the solutions of Maxwell’s equations for  $E(z)$  and  $H(z)$  in the  $p$ -th cell are

$$\begin{aligned} E_y(z), H_y(z) &= a_p e^{ik_1(z-pd)} + b_p e^{-ik_1(z-pd)} \\ &= c_p e^{ik_2(z-pd)} + d_p e^{-ik_2(z-pd)} \\ &= e_p e^{ik_1(z-pd)} + f_p e^{-ik_1(z-pd)}, \end{aligned} \quad (4)$$

in regions  $pd < z < pd + d_t$ ,  $pd + d_t < z < pd + d_t + d_2$  and  $pd + d_t + d_2 < z < (p+1)d$  respectively. Of course, the coefficients  $(a_p, b_p)$ ,  $(c_p, d_p)$ , and  $(e_p, f_p)$  differ for TE and TM waves.

The transfer matrix,  $\mathcal{M}$ , is defined so that

$$\begin{pmatrix} a_{p+1} \\ b_{p+1} \end{pmatrix} = \mathcal{M} \begin{pmatrix} a_p \\ b_p \end{pmatrix} \equiv \begin{pmatrix} A & B \\ B^* & A^* \end{pmatrix} \begin{pmatrix} a_p \\ b_p \end{pmatrix}. \quad (5)$$

Matching the fields in eq. (4) and their derivatives (the derivatives divided by  $n^2$ ) for TE (TM) waves, one finds

$$\begin{aligned} A^{\text{TE}} &= e^{ik_1 d_1} \left( \cos k_2 d_2 + \frac{i}{2} \left( \frac{k_1}{k_2} + \frac{k_2}{k_1} \right) \sin k_2 d_2 \right), \\ B^{\text{TE}} &= \frac{i}{2} e^{ik_1(d_1-2d_t)} \left( \frac{k_2}{k_1} - \frac{k_1}{k_2} \right) \sin k_2 d_2, \end{aligned} \quad (6)$$

and

$$\begin{aligned} A^{\text{TM}} &= e^{ik_1 d_1} \left[ \cos k_2 d_2 + \frac{i}{2} \left( \frac{n_1^2 k_2}{n_2^2 k_1} + \frac{n_2^2 k_1}{n_1^2 k_2} \right) \sin k_2 d_2 \right], \\ B^{\text{TM}} &= \frac{i}{2} e^{ik_1(d_1-2d_t)} \left( \frac{n_1^2 k_2}{n_2^2 k_1} - \frac{n_2^2 k_1}{n_1^2 k_2} \right) \sin k_2 d_2. \end{aligned} \quad (7)$$

Once these are known, the Bloch waves of the 1D crystal are determined by the eigenvalue equation

$$\begin{pmatrix} a_{p+1} \\ b_{p+1} \end{pmatrix} = \lambda \begin{pmatrix} a_p \\ b_p \end{pmatrix} = \mathcal{M} \begin{pmatrix} a_p \\ b_p \end{pmatrix}, \quad (8)$$

and therefore the  $\lambda$  satisfy

$$(A - \lambda)(A^* - \lambda) - |B|^2 = 0. \quad (9)$$

Using that  $\det \mathcal{M} = |A|^2 - |B|^2 = 1$ , one finds

$$\lambda_{\pm} = \text{Re}(A) \pm \sqrt{\text{Re}(A)^2 - 1}, \quad (10)$$

and eigenvectors

$$\begin{pmatrix} a \\ b \end{pmatrix} \propto \begin{pmatrix} B \\ \lambda_{\pm} - A \end{pmatrix}. \quad (11)$$

In the bandgaps  $\lambda_{\pm}$  are real since  $|\text{Re}A| > 1$ . In contrast, in allowed bands  $\lambda_{\pm} = e^{\pm i\phi}$  with  $\phi$  real. The bandgap boundaries are at  $\text{Re}A = \pm 1$ . Furthermore, from eq. (10)  $\lambda_- \lambda_+ = 1$ . For surface states one chooses the  $\lambda$  that corresponds to a damped Bloch wave when  $z \rightarrow +\infty$ . It must fulfill the condition  $|\lambda| < 1$ , and is  $\lambda_-$  ( $\lambda_+$ ) when  $\text{Re}(A) > 1$  ( $< -1$ .) For simplicity we write it simply as  $\lambda$  from here on.

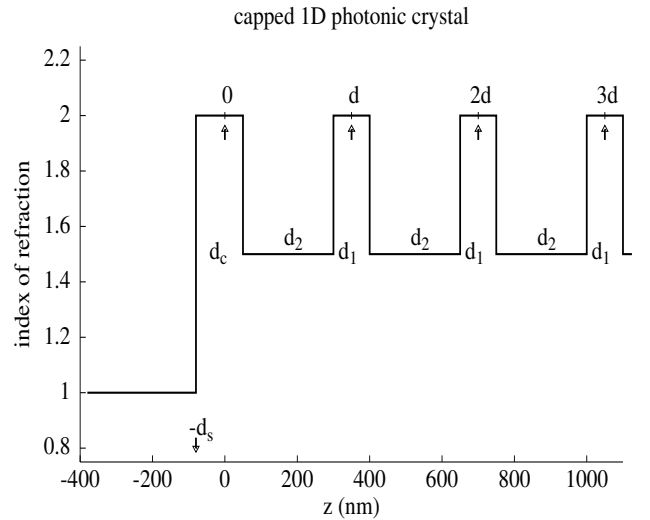


FIG. 1: Sketch of a typical 1D PC, for the case used in calculations ( $n_1 = 2.0$ ,  $d_1 = 100$  nm,  $n_2 = 1.5$ ,  $d_2 = 250$  nm,) A symmetric unit cell was chosen, and  $d_s = 80$  nm.

### A. Brewster Points

Brewster points exist only for TM waves, and require  $\text{Re } A^{\text{TM}} = \pm 1$ . From eq. (7) we find that

$$\begin{aligned} \text{Re } A^{\text{TM}} &= \cos k_1 d_1 \cos k_2 d_2 \\ &- \frac{1}{2} \left( \frac{n_1^2 k_2}{n_2^2 k_1} + \frac{n_2^2 k_1}{n_1^2 k_2} \right) \sin k_1 d_1 \sin k_2 d_2. \end{aligned} \quad (12)$$

It can be easily checked that a Brewster point occurs when

$$\frac{k_1}{n_1^2} = \frac{k_2}{n_2^2} \quad \text{and} \quad k_1 d_1 + k_2 d_2 = m\pi, \quad (13)$$

with  $m = 1, 2, \dots$  an integer which we assume to be the bandgap index. The first of these equations determines  $\beta$ . In particular, we have

$$\frac{\sqrt{n_1^2 - \beta^2}}{n_1^2} = \frac{\sqrt{n_2^2 - \beta^2}}{n_2^2} \quad (14)$$

and, as a result,

$$\beta_{Br} = \frac{n_1 n_2}{\sqrt{n_1^2 + n_2^2}}. \quad (15)$$

The second of equations (13) then fixes the value of  $k$  to be

$$k_{Br} = \frac{m\pi}{d_1 \sqrt{n_1^2 - \beta^2} + d_2 \sqrt{n_2^2 - \beta^2}}. \quad (16)$$

For our reference case, see Fig. 1, we find that  $\beta_{Br} = 1.2$ ,  $k_{Br} = 0.00816 \text{ nm}^{-1}$  when  $m = 1$  (first bandgap). A numerical determination of the bandgap boundaries confirms that the gap width shrinks to zero at this point.

### III. SURFACE TM WAVES

Most derivations are analogous to TE case, see Ref. [9]. The magnetic field of a surface TM wave is written as

$$H_y(z) = a_s e^{ik_1 z} + b_s e^{-ik_1 z}, \quad (17)$$

when  $-d_s < z < 0$  and

$$H_y(z) = b_v e^{q_0 z}, \quad (18)$$

with  $q_0 = +k\sqrt{\beta^2 - n_0^2}$ , when  $z < -d_s$ . Using the boundary conditions, we obtain the exact dispersion relation  $k = k(\beta)$  for TM surface waves by solving

$$\begin{aligned} \frac{q_0}{k_1} \frac{n_1^2}{n_0^2} &= -i \frac{\lambda^{\text{TM}} - A^{\text{TM}} - \tilde{B}^{\text{TM}}}{\lambda^{\text{TM}} - A^{\text{TM}} + \tilde{B}^{\text{TM}}}, \\ \tilde{B}^{\text{TM}} &\equiv e^{-2ik_1 d_s} B^{\text{TM}}. \end{aligned} \quad (19)$$

This equation must be solved numerically, and we will refer to the solutions thereby obtained as “exact”. We

note that the ratio  $q_0/k_1$  depends only on  $\beta$ , and is independent of  $k$ . Furthermore, from eq. (9) one has that  $\lambda - A$ ,  $B$  and  $\tilde{B}$ , have the same modulus and therefore eq. (19) becomes:

$$\frac{q_0}{k_1} \frac{n_1^2}{n_0^2} = -i \frac{e^{i\theta_{\lambda-A}} - e^{i\theta_{\tilde{B}}}}{e^{i\theta_{\lambda-A}} + e^{i\theta_{\tilde{B}}}} = \tan \left( \frac{\theta_{\lambda-A} - \theta_{\tilde{B}}}{2} \right), \quad (20)$$

where we have defined

$$\theta_{\lambda-A} \equiv \arg(\lambda - A) \quad , \quad \theta_{\tilde{B}} = \arg(\tilde{B}). \quad (21)$$

To determine the latter, we note that

$$\begin{aligned} c_- &\equiv \frac{n_1^2 k_2}{n_2^2 k_1} - \frac{n_2^2 k_1}{n_1^2 k_2} \\ &= \frac{(n_1^2 - n_2^2)(n_1^2 n_2^2 - \beta^2(n_1^2 + n_2^2))}{n_1^2 n_2^2 \sqrt{(n_1^2 - \beta^2)(n_2^2 - \beta^2)}}, \end{aligned} \quad (22)$$

appearing in eq. (7) can have either sign. In fact we expect that the sign will change when  $\beta$  runs from  $n_0 = 1$  to  $n_2$ . We therefore write

$$\theta_{\tilde{B}} = \frac{\pi}{2} + kn_{1\beta}(d_1 - 2d_c) + \phi_s \quad (23)$$

with  $\phi_s$  chosen to be 0 or  $-\pi$  depending on the sign of  $c_- \sin(k_2 d_2)$ . As shown in Ref. [10], this sign is characteristic of each bandgap, unless the width shrinks to zero in either an optical hole [10] or a Brewster point. Returning to eq. (20), we can now write  $\theta_{\lambda-A}$  explicitly as

$$\theta_{\lambda-A}(k) = 2\Theta(\beta) + kn_{1\beta}(d_1 - 2d_c) + \phi_s + \frac{\pi}{2} + 2\pi\nu \quad (24)$$

with  $\nu = 0, \pm 1, \pm 2, \dots$ , and where we have defined

$$\Theta(\beta) \equiv \tan^{-1} \left( \frac{n_1^2}{n_0^2} \sqrt{\frac{\beta^2 - n_0^2}{n_1^2 - \beta^2}} \right). \quad (25)$$

Note that all dependence on  $k$  on the r.h.s. of eq. (24) is explicit in the second term. Note also that in taking the inverse tangent we have introduced a contribution of  $+2\pi\nu$  on the r.h.s. This term was discussed at length in Ref. [9], so here we will discuss only the solutions with  $\nu = 0$ .

There is no simple analytic form for  $\theta_{\lambda-A}$  as a function of  $k$ , so numerical methods must be used to solve eq. (24). However, the results can be better understood using a simple graphical approach. In Fig. 2 we plot  $\theta_{\lambda-A}(k)$  (continuous line), and the r.h.s. of eq. (24) for a chosen set of  $d_c$ 's (dashed lines). One sees that  $\theta_{\lambda-A}$  increases from  $-\pi/2$  to  $\pi/2$  as  $k$  ranges from the lower to the upper first bandgap boundaries. In a more general context, this property has been shown to hold in Ref. [12]. For a given  $d_c$ , the intersection of the corresponding straight line with the continuous line determines the solution for  $k$ . As the graph shows, when  $d_c$  decreases,  $k$  increases. The values of  $d_c$  for which a solution can be found will therefore be

bounded by those corresponding to the r.h.s. of eq. (24) where it crosses  $\theta_{\lambda-A} = \pm\pi/2$ . That condition leads to

$$\begin{aligned} d_{c,min} &= \frac{d_1}{2} + \frac{1}{k_R n_{1,\beta}} \left( \Theta(\beta) + \frac{\phi_s}{2} \right), \\ d_{c,max} &= \frac{d_1}{2} + \frac{1}{k_L n_{1,\beta}} \left( \Theta(\beta) + \frac{\phi_s}{2} + \frac{\pi}{2} \right). \end{aligned} \quad (26)$$

In the example shown in Fig. 2, one finds  $d_{c,min} = 21$  nm and  $d_{c,max} = 134$  nm (For this example,  $\phi_s = -\pi$  and  $\beta > \beta_{Br}$ ).

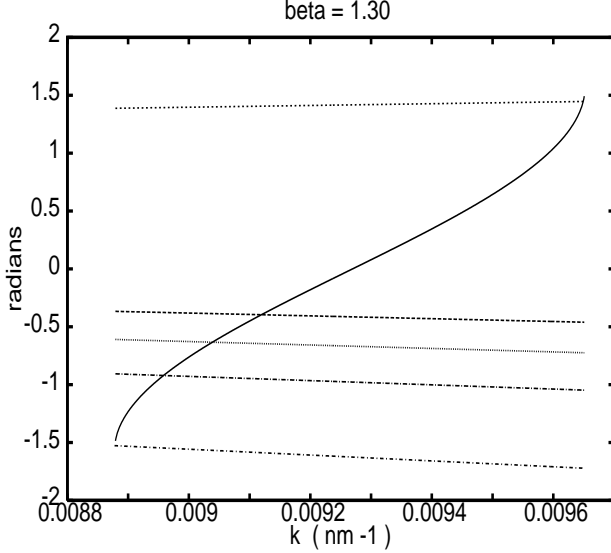


FIG. 2: Graphical solution of eq. (24) for  $n_0 = 1$ ,  $n_1 = 2$ ,  $d_1 = 100$  nm,  $n_2 = 1.5$ ,  $d_2 = 250$  nm, and  $\beta = 1.3$ . Continuous line:  $\theta_{\lambda-A}$ ; dashed lines: r.h.s. for several values, from top to bottom,  $d_c = 0.25, 0.90, 0.99, 1.01$  and  $1.33d_1$ .

The same expressions also apply when  $\beta < \beta_{Br}$ , but then  $\phi_s = 0$ . If we choose  $\beta = 1.01$ , the limits are  $d_{c,min} = 75$  nm and  $d_{c,max} = 134$  nm. The graphical solutions are now shown in Fig. 3.

To proceed further in the analysis of the SEW solutions requires values for the band edges  $k_L$ ,  $k_R$  for a given  $\beta$ . These can be obtained from our semiclassical approximation [8]. In Ref. [9] we found very accurate analytic approximations for the TE bandgaps. Formally analogous expressions hold for TM bandgap boundaries, and their accuracy is also excellent. We have also shown that the semiclassical theory allows one to derive a good approximate expression for the argument of  $\lambda - A$ . In the first bandgap, it is

$$\theta_{\lambda-A}^{(e)} = \sin^{-1} \left( \frac{k - k_m}{w/2} \right) \quad (27)$$

with  $k_m \equiv (k_R + k_L)/2$  and  $w = k_R - k_L$ .

In Fig. 4 we compare the exact value and the above approximation for  $\theta_{\lambda-A}$  for several values of  $\beta$  ranging from

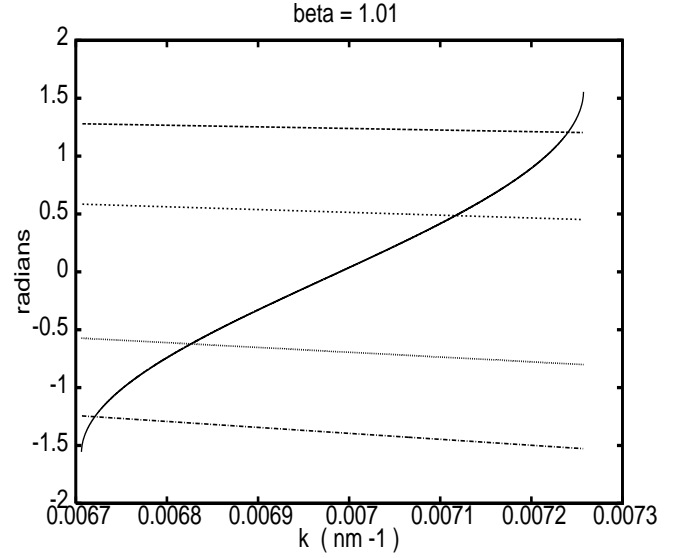


FIG. 3: Graphical solution of eq. (24) for  $n_0 = 1$ ,  $n_1 = 2$ ,  $d_1 = 100$  nm,  $n_2 = 1.5$ ,  $d_2 = 250$  nm, and  $\beta = 1.01$ . Continuous line:  $\theta_{\lambda-A}$ ; dashed lines: r.h.s. for several values, from top to bottom,  $d_c = 0.90, 1.20, 1.70$  and  $2.0d_1$ .

$n_0$  to  $n_2$ . For this example, the approximation is so good that on that scale one cannot distinguish between the exact and the approximate curves.

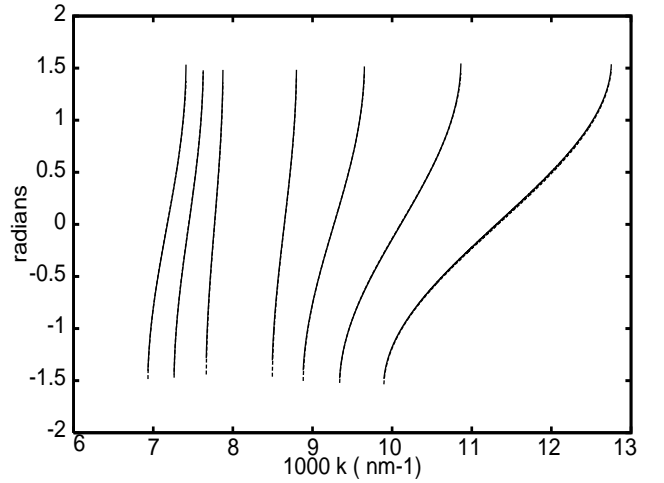


FIG. 4: Exact (continuous line) v.s. empirical approximation (dashed line) to the argument of  $\lambda - A$ . From left to right,  $\beta = 1.05, 1.1, 1.15, 1.25, 1.3, 1.35$  and  $1.4$ . We omitted the curves corresponding to the Brewster point at  $\beta_{Br} = 1.2$ .

### A. Approximate analytical solutions in the middle of the first bandgap.

SEW in the middle of a bandgap are of interest because the damping is strong, so most of the surface wave is confined very close to the surface. For momenta such that  $k - k_m \ll w$  one can make the simplification  $\sin^{-1}(2(k - k_m)/w) \simeq 2(k - k_m)/w$  and eq. (24) then gives

$$k \simeq \frac{\Theta(\beta) + k_m/w + \phi_s/2 + \pi(\nu + 1/4)}{1/w + n_{1\beta}(d_c - d_1/2)}. \quad (28)$$

The dependence of  $k$  on  $d_c$ ,  $\beta$  and  $d_1$  is now transparent. The role of the bandgap parameters  $k_m$  and  $w$  can also be easily discussed. Fig. 5 shows the accuracy of this approximation when  $\beta > \beta_{Br}$ .

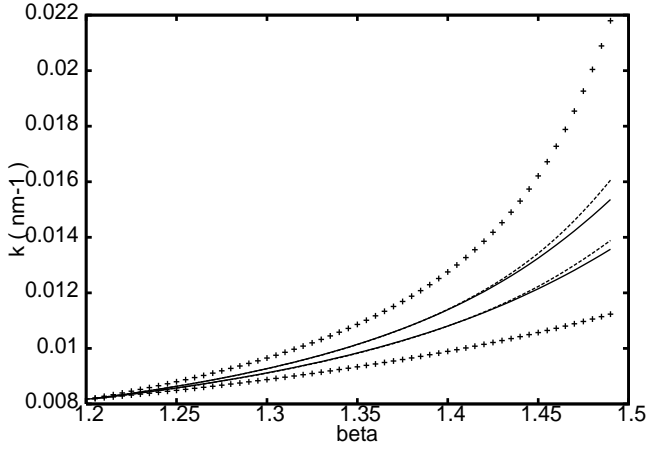


FIG. 5: Dispersion relation  $k = k(\beta)$  when  $d_c = 0.75 d_1$ ,  $0.90 d_1$ . Continuous line: exact solution of eq. (19). Dotted line: linear approximation, eq. (28). Crosses: first bandgap boundaries.

### B. Approximate solutions near the bandgap boundaries.

Here we discuss solutions near the upper bandgap boundary, but similar approximations can be developed for the lower boundary, as in Ref. [9]. When  $k$  is slightly below  $k_R = k_m + w/2$ , it is convenient to introduce  $\zeta > 0$  via

$$k - k_m = \frac{w}{2}(1 - \zeta). \quad (29)$$

Then,

$$\sin^{-1}\left(\frac{k - k_m}{w/2}\right) \simeq \frac{\pi}{2} - \sqrt{2\zeta} = \frac{\pi}{2} - 2\sqrt{\frac{k_R - k}{w}}. \quad (30)$$

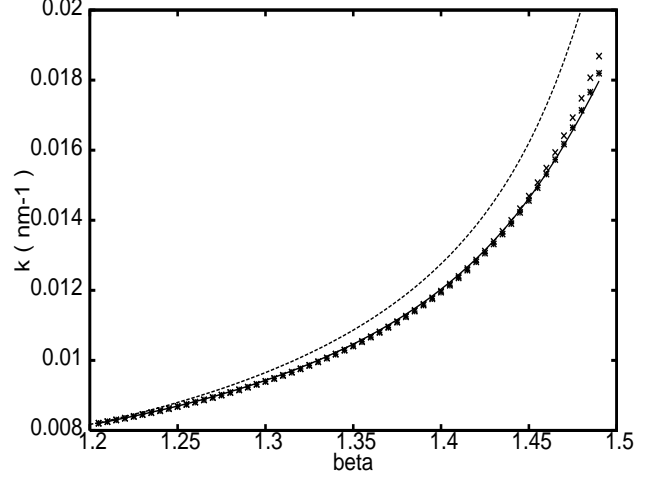


FIG. 6: Dispersion relation  $k = k(\beta)$  when  $d_c = 0.60 d_1$ . Exact solution (continuous line) v.s. approximations: Crosses: eq. (33); stars: eq. (34). The dashed line is the upper boundary of the first bandgap.

Inserting this into eq. (24) gives

$$2\sqrt{\frac{k_R - k}{w}} + p(k_R - k) = \Lambda \quad (31)$$

with

$$p \equiv n_{1\beta}(2d_c - d_1) \quad \Lambda \equiv -2\Theta - \phi_s + k_R p. \quad (32)$$

Solving for  $k_R - k$ , we obtain

$$k = k_R - \frac{1}{p^2} \left( -\frac{1}{\sqrt{w}} + \sqrt{\frac{1}{w} + p\Lambda} \right)^2. \quad (33)$$

which is the desired solution,  $k = k(\beta)$ , near the upper bandgap boundary. Fig. 6 shows an example of the accuracy of this expression. Furthermore, when  $p\Lambda$  is small compared to  $1/w$  one can expand and find

$$k = k_R - \frac{1}{4}w\Lambda^2, \quad (34)$$

which again manifests the dependence of  $k$  on  $d_c$  and  $w$ , and allows one to construct  $k = k(\beta)$  very easily. Fig. 6 shows again the validity of this approximation.

#### IV. FIRST AND SECOND SEMICLASSICAL APPROXIMATIONS

The transfer matrix relates the amplitudes for transmission  $t_B$  and reflection  $r_B$  of a single cell as

$$\begin{pmatrix} t_B \\ 0 \end{pmatrix} = \mathcal{M} \begin{pmatrix} 1 \\ r_B \end{pmatrix}. \quad (35)$$

Comparing to eq. (5),  $A = 1/t_B^*$  and  $B = -r_B^*/t_B^*$ . In the first approximation, the expressions for  $r_B$  and  $t_B$  are given in Refs. [6, 7] for TE waves and in Ref. [8] for TM waves. In particular, we have

$$\begin{aligned} r_B^{(1)} &= \frac{-s_q^* \sinh(\gamma_1 d)}{\gamma_1 \cosh(\gamma_1 d) - i\delta_q \sinh(\gamma_1 d)}, \\ t_B^{(1)} &= \frac{(-)^q \gamma_1}{\gamma_1 \cosh(\gamma_1 d) - i\delta_q \sinh(\gamma_1 d)}, \end{aligned} \quad (36)$$

where the coefficients  $s_q$  differ of course for TE and TM waves. For a photonic crystal with a symmetric cell,  $d_1 = 2d_t$ , they take the form

$$s_q^{\text{TE}} = -\frac{i}{d} \ln \left[ \frac{k_1}{k_2} \right] e^{-iq\pi} \sin \left[ \frac{d_2}{d} [q\pi + (k_2 - k_1)d_1] \right], \quad (37)$$

$$s_q^{\text{TM}} = -\frac{i}{d} \ln \left[ \frac{k_1 n_2^2}{k_2 n_1^2} \right] e^{-iq\pi} \sin \left[ \frac{d_2}{d} [q\pi + (k_2 - k_1)d_1] \right]. \quad (38)$$

The parameter  $\delta_q$  is the detuning from the  $q$ -th Bragg resonance  $k_q$ ,  $q = 1, 2, \dots$  and the well-known Bragg condition for constructive interference is

$$k_q = \frac{\pi}{n_{av}d} q, \quad \delta_q = kn_{av} - \frac{\pi}{d} q. \quad (39)$$

The parameter  $\gamma_1$  appearing in eqs. (36) is defined as  $\gamma_1 \equiv \sqrt{|s_q|^2 - \delta_q^2}$ . Then, for the elements of the transfer matrix in the first approximation of the semiclassical coupled wave theory, we obtain

$$A^{(1)} = (-)^q \left( \cosh \gamma_1 d + i \frac{\delta_q}{\gamma_1} \sinh \gamma_1 d \right), \quad (40)$$

$$B^{(1)} = (-)^q \frac{s_q}{\gamma_1} \sinh \gamma_1 d. \quad (41)$$

Inserting  $\text{Re}(A^{(1)})$  into eq. (11), we find that  $\lambda^{(1)} = (-)^q e^{-\gamma_1 d}$ , where  $\lambda^{(1)}$  is the first semiclassical approximation to the eigenvalue of the damped Bloch wave.

The second approximation introduced in Refs. [7, 8] leads to similar expressions for the elements of the transfer matrix:

$$A^{(2)} = (-)^q \left[ \cosh \gamma_2 d + i \frac{[(1 + |u|^2)\eta_q - 2\text{Im}(s_q u^*)]}{(1 - |u|^2)\gamma_2} \sinh \gamma_2 d \right], \quad (42)$$

$$B^{(2)} = (-)^q \frac{s_q - 2i\eta_q u - s_q^* u^2}{(1 - |u|^2)\gamma_2} \sinh \gamma_2 d, \quad (43)$$

where  $\gamma_2 \equiv \sqrt{|s_q|^2 - \eta_q^2}$ ,  $\eta_q = \delta_q - ic_2$  and

$$c_2 = \frac{id}{2\pi} \sum_{m \neq q=-\infty}^{m=+\infty} \frac{|s_m|^2}{m - q - \delta_q d/\pi}, \quad (44)$$

$$u = -\frac{id}{2\pi} \sum_{m=-\infty, m \neq q}^{m=+\infty} \frac{s_m}{m - q - \delta_q d/\pi}. \quad (45)$$

The eigenvalue of the damped wave is  $\lambda^{(2)} = (-)^q e^{-\gamma_2 d}$ .

Inserting  $A^{(1,2)}$  and  $B^{(1,2)}$  into eqs. (19), one finds the corresponding predictions for  $k = k(\beta)$  of TM surface waves. Selected results are shown in Fig. 7. As can be seen, the second approximation gives excellent agreement with the exact dispersion relation within the range of validity  $\beta < n_2$  of the semiclassical coupled wave theory, for the problem at hand.

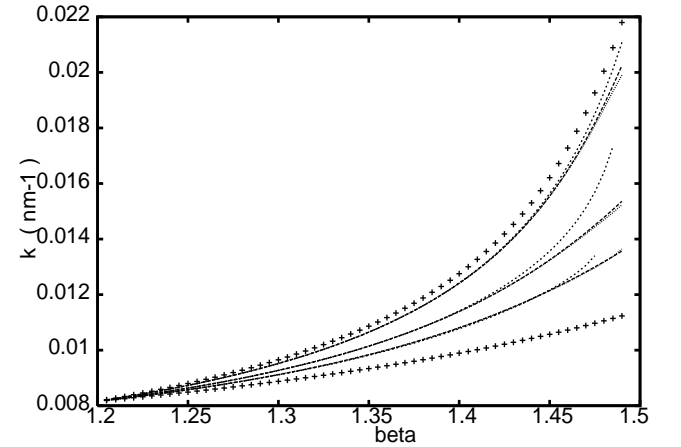


FIG. 7:  $k = k(\beta)$  curves for TM waves in the first bandgap for  $d_c = 50, 75$  and  $90$  nm; continuous lines: exact solutions; long dashes: first semiclassical approximations; short dashes: second semiclassical approximation; crosses: bandgap boundaries

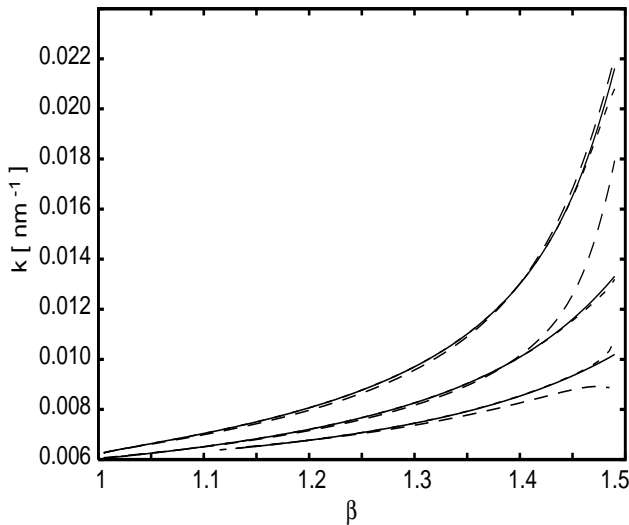


FIG. 8:  $k = k(\beta)$  curves for TE waves in the first bandgap for  $d_c = 25, 50$  and  $75$  nm; continuous lines: exact solutions; long dashes: first semiclassical approximations; short dashes: second semiclassical approximation. The latter curves are so close to the exact ones that the difference can be seen only when  $\beta > 1.45$ .

As shown in Ref. [9], the dispersion relation  $k = k(\beta)$  for TE surface waves is found by solving

$$\frac{q_0}{k_1} = -i \frac{\lambda^{\text{TE}} - A^{\text{TE}} - \tilde{B}^{\text{TE}}}{\lambda^{\text{TM}} - A^{\text{TE}} + \tilde{B}^{\text{TE}}}, \quad \tilde{B}^{\text{TE}} \equiv e^{-2ik_1 d_s} B^{\text{TE}}. \quad (46)$$

In Fig. 8 we compare the exact and semiclassical results for  $k = k(\beta)$ , choosing three thicknesses of the cap layer  $d_c = 25, 50$  and  $75$  nm. The first approximation becomes inaccurate when  $\beta$  exceeds  $1.4$ , but gives accurate results up to that value. The second approximation is so close to the exact values that one can see the difference only for values of  $\beta$  very close to the critical value  $\beta = n_2 = 1.5$ . Beyond that, our semiclassical approximation cannot be applied, since  $k_2$  becomes imaginary.

### Acknowledgments

We are grateful to NSERC-Canada for Discovery Grant RGPIN-3198 (DWLS), and to DGES-Spain for continued support through grants BFM2001-3710 and FIS2004-03156 (JM).

- 
- [1] E. Moreno, L. M. Moreno, and F. J. Garcia-Vidal, “Enhanced transmission and beaming of light via photonic crystal surface modes”, *Phys. Rev. B* **69**, 121402(R) (2004).
  - [2] P. Kramper, M. Agio, C. M. Soukoulis, A. Bimer, F. Müller, R. Wehrspohn, U. Gösele, and V. Sandogh-dar, “Highly directional emission from photonic crystal waveguides of subwavelength width”, *Phys. Rev. Lett.* **92**, 113903 (2004).
  - [3] H. Kogelnik, “Coupled wave theory for thick hologram gratings”, *Bell Syst. Tech. J.* **48**, 2909 (1969).
  - [4] A. Yariv and P. Yeh, *Optical Waves in Crystals*, John Wiley & Sons, New York, 1984.
  - [5] P. Yeh, *Waves in Layered Media*, John Wiley & Sons, New York, 1988.
  - [6] S. Y. Karpov and S. N. Stolyarov, “Propagation and transformation of electromagnetic waves in one dimensional periodic structures”, *Usp. Fiz. Nauk* **163**, 63 (1993) [*Phys. Usp.* **36** 1 (1993)].
  - [7] G. V. Morozov, D. W. L. Sprung, and J. Martorell, “Semiclassical coupled-wave theory and its applications to TE waves in one-dimensional photonic crystals”, *Phys. Rev. E* **69**, 016612 (2004).
  - [8] G. V. Morozov, D. W. L. Sprung, and J. Martorell, “Semiclassical coupled wave theory for TM waves in one-dimensional photonic crystals”, *Phys. Rev. E* **70**, 016606 (2004).
  - [9] J. Martorell, D. W. L. Sprung, and G. V. Morozov, “Surface TE waves on 1D photonic crystals”, *Journal of Optics A: Pure and Applied Optics* **8**, 630 (2006).
  - [10] J. A. Gaspar-Armenta and F. Villa, “Band-structure properties of one-dimensional photonic crystals under the formalism of equivalent systems”, *J. Opt. Soc. Am. B* **21**, 405 (2004).
  - [11] R. Petit, *Electromagnetic theory of gratings*, Springer Verlag, Berlin Heidelberg, 1980.
  - [12] D. W. L. Sprung, G. V. Morozov, and J. Martorell, “Geometrical approach to scattering in one dimension”, *J. Phys. A: Math. Gen.* **37**, 1861 (2004).